Corona onset voltage at 60 Hz and at high frequency for an isolated, cylindrical monopole

Corona Onset Voltage at 60 Hz and at High Frequency for an Isolated Cylindrical Monopole

William O. Price, *Member, IEEE*, John Drapala, *Member, IEEE*, David V. Thiel, *Senior Member, IEEE*, and Robert G. Olsen, *Fellow, IEEE*

***Abstract*—Corona on electrified conductors (power lines, transmission lines, and antennas) is a significant source of electromagnetic interference to aircraft. The Townsend integral, which describes breakdown in low-frequency nonuniform fields, is derived from the electron continuity equation. Predictions of corona onset are made using published formulas for net ionization. Measurements of 60-Hz corona onset for an isolated cylindrical monopole are compared with predictions. A corona onset criterion, which describes breakdown in nonuniform radio-frequency fields, is also derived from the electron continuity equation. Measurements of corona onset at 300 MHz for the same isolated cylindrical monopole are compared with predictions. The results confirm that the derived breakdown criteria are good predictors of corona onset both at 60 Hz and 300 MHz for cylindrical geometries in the range $0.1 \leq rp \leq 10$ cm·torr. A discussion of the transition frequency between power frequency and high-frequency corona onset is also included.**

***Index Terms*—Aircraft, antennas, corona, cylindrical monopole, diffusion equations, electromagnetic interference, electron continuity equation, ionization.**

I. Introduction

FROM the first day of manned flight until now, electrical discharges have played a significant role in aviation incidents and accidents. Best known are the lightning and static discharges that have each claimed their victims;[1] precipitation static has interfered with flight-critical communications and navigation.[2] Less known are the corona discharges and arcing that disable electric power and radio-frequency (RF) systems in the rarefied air of the flight regime. While the literature on lightning and precipitation static is relatively large, that on electrical and RF corona in flight is sparse. In this paper, we relate a general theory of corona onset that spans both power frequencies and RFs in the regime of flight. We report the results of experimental measurements of corona onset for a cylindrical monopole at 60 Hz and 300 MHz. We extend previous work [2], [3] with a discussion of the frequency at which one phenomenon might change to the other.

A. Technical Approach and Assumptions

Corona is a local phenomenon. A necessary condition for its onset is an electric field strong enough in a region large enough to support an exponential avalanche of electrons by ionizing collision. Since the electric fields very near power lines, RF transmission lines, and antennas are typically nonuniform, the onset of corona will be dependent on both the strength of the field at the surface of the conductor and the degree of field nonuniformity.

If one describes an arbitrarily convex, conductive surface by a minimum radius of curvature, then the divergence of the local electric field adjacent to the surface will fall within two extremes. The first is the spherical with two equal orthogonal radii of curvature; the second is the cylindrical with only one finite radius of curvature. All other things being equal, the lowest threshold of corona onset, as measured by surface electric field intensity, will be associated with the least divergent electric field. Thus, our study has focused on corona onset of cylindrical conductors.

Furthermore, since other conductors near the region of ionization induce electron loss in addition to diffusion and drift, and raise the threshold of corona onset, we have analyzed breakdown for an isolated, cylindrical monopole.

B. Low-Frequency Corona

About the turn of the last century, Townsend published his theory of the electron avalanche as the explanatory mechanism of electrical breakdown in gases [4]. For breakdown in uniform fields, Townsend stated his well-known law

$$i = i_0\, e^{\alpha x} \tag{1}$$

where i is the current at the anode, i_0 is the primary current, x is the distance between the parallel-plate electrodes, and α is the electron ionization coefficient, a strong function of electric field intensity.

Manuscript received November 13, 2007.

W. O. Price is with the Airborne Warning Systems Division, Boeing Company, Seattle, WA 98124 USA, and also with Griffith University, Brisbane, Qld. 4111, Australia (e-mail: william.o.price@boeing.com).

J. Drapala is with the Airborne Warning Systems Division, Boeing Company, Seattle, WA 98124 USA (e-mail: john.drapala@boeing.com).

D. V. Thiel is with the Griffith School of Engineering, Griffith University, Brisbane, Qld. 4111, Australia.

R. G. Olsen is with the College of Engineering and Architecture, Washington State University, Pullman, WA 99164 USA.

Color versions of one or more of the figures in this paper are available online at http://ieeexplore.ieee.org.

Digital Object Identifier 10.1109/TEMC.2008.926805

[1] Among the earliest reports are those of the German Naval dirigible L10 that crashed on September 3, 1915, at the mouth of the Elbe with 19 killed after a lightning attachment, and the German Naval dirigible SL9 that crashed and burned on March 30, 1917, in the Baltic sea with 23 people killed after lightning attachment. The Hindenburg tragedy may have resulted from an inadvertent static discharge while mooring. An untold number of fixed-wing aircraft succumbed to lightning before Western governments kept adequate records. Loss of life and aircraft by lightning extends into the present era.

[2] When the U.S. Government required communication and navigation radios in commercial aircraft in the 1930s, the phenomenon was termed "radio range variation" [1]. It was almost ten years before the cause of the interference was correctly identified and a reasonable mitigation implemented. To this day, precipitation static poses a significant hazard to flight.

Loeb [5] attributed a modification of the avalanche expression for nonuniform electric fields to Townsend [6]

$$i = i_0\, e^{\int \alpha\, dx}. \tag{2}$$

Phillips *et al.* [7], citing McAllister and Pedersen [8], state that "since the integral of (2) dominates the corona onset condition and that all methods for calculating corona onset are to some extent empirical, the corona onset condition can be written as ..."

$$K = \exp\left[\int_0^d \frac{(\alpha - \eta)}{p} dx\right] \tag{3}$$

where η is the electron attachment coefficient, d is the ionization boundary (where $\alpha = \eta$), and $\boldsymbol{K}$ is a constant determined by fitting (3) to experimental data. Using expressions for α and η developed by Sarma and Janischewskyj [9], Pedrow and Olsen [10] calculated $\boldsymbol{K}$ to be 3500.

The Townsend integral seems to have been developed heuristically. Nowhere did Townsend derive the integral from more fundamental physics, but, it appears, from the concept of the electron avalanche, an obviously exponential phenomenon.

C. High-Frequency Corona

After the British invention of the cavity magnetron in 1940 came a series of developments on both sides of the Atlantic that increased the power and efficiency of microwave devices by orders of magnitude [11]. It soon became apparent that a limit to further development was the electrical breakdown of air in cavities and transmission lines.

As the jet age dawned and high-power communications and sensors found their way onto air vehicles, a new problem arose: the breakdown of air around antennas. The onset of corona in high-power RF systems often resulted in the loss of function, interference to other systems, and damage. The earliest report of voltage breakdown of airborne antennas is found in the U.S. Army's records of German scientific research before World War II [12].[3] Just after the war, Posin [13] related that "[d]uring the course of the radar work at the Radiation Laboratory, M.I.T., serious problems were posed by undesired sparking of radiofrequency components when high power emanated from magnetrons." In 1948, Herlin and Brown [14]–[16] summarized the work at the Radiation Laboratory and published a diffusion theory of high-frequency gas breakdown that accurately predicted breakdown in coaxial structures and cylindrical cavities. The most significant work in the three decades after the war was performed by Brown *et al.* at the Massachusetts Institute of Technology [17], [18], Chown *et al.* at Stanford Research Institute [19]–[25], and Fante *et al.* at Aviation Corporation (AVCO) [26]–[34].

The two phenomena—power frequency and RF corona—are markedly different. They occur at different electric field intensities; the corona produced by high-frequency excitation is brighter than that produced by power frequency excitation; the two phenomena occur in very different systems. On the other hand, both are the result of ionization by electron collision. We will argue that both phenomena are explained by the same theory and that the notable differences are due to different electron loss mechanisms.

II. Theory

In his 1965 paper on microwave breakdown, Fante [26, Appendix] derived the electron continuity equation from the Boltzmann transport equation

$$\frac{\partial n}{\partial t} = -\nabla \cdot \boldsymbol{\Gamma} + (\nu_i - \nu_a)\, n \tag{4}$$

where n is the electron density, $\boldsymbol{\Gamma}$ is the electron current density, ν_i and ν_a are the electron ionization and attachment frequencies, respectively.[4] The electron current density is

$$\boldsymbol{\Gamma} = \langle \boldsymbol{V} \rangle\, n - \mu \boldsymbol{E} n - \nabla D n \tag{5}$$

where $\boldsymbol{V}$ is the velocity of the gas, μ is the electron mobility, and D is the diffusion coefficient. The three terms on the right-hand side of (5) are, respectively, *convection*, *drift*, and *diffusion*. For the purposes of this study, we have excluded convection because most antennas of interest are behind radomes and in relatively still air. Herlin and Brown [14] state that in a microwave discharge, in which the excitation frequency is relatively large, drift is oscillatory and does not contribute to electron transport. Thus, the only significant loss mechanism is diffusion. However, at lower frequencies, drift becomes the dominant loss mechanism because electron motion during a half-cycle is large enough to remove electrons from the region of ionization.

A. Low-Frequency Corona

When electron drift is the dominant loss mechanism, then

$$\boldsymbol{\Gamma} = \mu \boldsymbol{E} n \tag{6}$$

and (4) becomes

$$\frac{\partial n}{\partial t} = -\nabla \cdot (-\mu \boldsymbol{E} n) + \nu n \tag{7}$$

where ν is the net electron ionization frequency and represents the difference between ionization and attachment frequencies

$$\nu = \nu_i - \nu_a. \tag{8}$$

The criterion for corona onset corresponds to the right-hand side of (7) becoming positive in the vicinity of the monopole (see the Appendix). The electron continuity equation may be solved by a separation of variables. Let

$$n(r, t) = n_r(r) n_t(t) \tag{9}$$

and the solution to the left-hand side of (7) becomes

$$n_t(t) = e^{\boldsymbol{\lambda} t}. \tag{10}$$

[3] Mehlhardt's report dates back to 1937, well before the introduction of airborne radar on German military aircraft in 1940 [11]. The reported breakdown probably had to do with high-frequency radio equipment.

[4] Though the Boltzmann transport equation describes all charged and neutral species, electrons dominate the breakdown of air because of their small mass and consequent ability to gain energy from the electric field. In this paper, only the contribution of electrons to the breakdown process is considered.

Nascent electron density will decay if λ is negative, but as λ becomes positive, electron density will grow exponentially and corona will form. Corona onset is described by the boundary between the two behaviors, $\lambda = 0$, and therefore, by the homogeneous ordinary differential equation

$$-\nabla \cdot (-\mu \boldsymbol{E} n_r) + \nu n_r = 0. \tag{11}$$

The electric field in the vicinity of an infinite cylindrical conductor is assumed to be predominantly radial [35]

$$E(r) \approx \frac{E_0 r_0}{r}, \qquad \text{for } r \geq r_0 \tag{12}$$

where E_0 is the electric field intensity at the surface of the monopole and r_0 is the radius of the monopole. Breakdown is described as

$$\frac{\mu}{r}\frac{\partial}{\partial r}\left(r\frac{E_0 r_0 n_r}{r}\right) + \nu n_r = 0 \tag{13}$$

or

$$\frac{n_r'}{n_r} = -\frac{\nu}{\mu E(r)}. \tag{14}$$

Integrating over r and choosing as the limits of integration the surface of the electrode and the ionization boundary, r_0 and r_1, respectively, we have

$$\frac{n_r(r_1)}{n_r(r_0)} = \exp\left[\int_{r_1}^{r_0} \frac{\nu}{\mu E(r)} dr\right]. \tag{15}$$

In order to be a useful predictor of corona onset, (15) is empirically calibrated [see (3)]. At sufficiently high pressures where electron motion under the influence of an electric field is described in terms of drift velocity and mobility, the net ionization frequency ν can be stated in terms of the ionization and attachment coefficients and drift velocity [36], [37]

$$\nu = (\alpha - \eta)\, v_d = (\alpha - \eta)\, \mu E \tag{16}$$

and so

$$n_r(r_1) = n_r(r_0) \exp\left[\int_{r_1}^{r_0} \frac{(\alpha - \eta)}{p} d(rp)\right] \tag{17}$$

which is the Townsend integral.

B. High-Frequency Corona

At high frequency where diffusion is the dominant electron loss mechanism

$$\Gamma = -\nabla D n_r \tag{18}$$

and (4) becomes

$$\frac{\partial n}{\partial t} = \nabla^2 D n + \nu n. \tag{19}$$

Since the diffusion coefficient D varies slowly as a function of the electric field intensity, i.e., $D\nabla^2 n >> n\nabla^2 D$, so

$$\frac{\partial n}{\partial t} \approx D\nabla^2 n + \nu n. \tag{20}$$

By separation of variables, the criterion for corona onset is described in cylindrical coordinates by the homogeneous ordinary differential equation

$$\frac{\partial^2 n_r}{\partial r^2} + \frac{1}{r}\frac{\partial n_r}{\partial r} + \frac{\nu}{D} n_r = 0 \tag{21}$$

which is Bessel's equation and has Bessel functions of integer order for solutions.

With appropriate boundary conditions, it is possible, in principle, to derive a nontrivial solution of (21) by the use of Cramer's rule. In several papers by Herlin and Brown [14]–[16], breakdown is calculated between coaxial cylinders. The walls of the inner and outer cylinders are natural boundaries where the electron density n_r vanishes. Fante *et al.* [32] derived similar breakdown conditions for coaxial cylinders but with the provision that the distance between them is so great that an ionization boundary may form (where $\nu = \nu_i - \nu_a = 0$). In such a case, there are three natural boundaries: the two cylinder walls and the ionization boundary where there is a singularity. Fante's approach was to form two problems with three boundaries. In the interior region where $\nu > 0$, $\nu \approx \nu_i$; in the outer region where $\nu < 0$, $\nu \approx \nu_a$. At the cylinder walls, the electron density vanishes, and at the ionization boundary, the solutions and their first derivatives are set equal to each other. By this means, Fante calculated the breakdown criteria to be in good agreement with experimental results. As the outer boundary becomes very large or infinite, the solution describes corona onset for an isolated monopole.

If one uses proper variables, i.e., *E/p* in volts per centimeter torr as a function of $\rho = rp$ in centimeter torr, where E is the electric field intensity, p is the pressure, and r is the radius, and further, if ρ_0 describes the surface of the cylindrical monopole, ρ_1 the ionization boundary, and ρ_2 an arbitrarily large outer boundary at which the electron density vanishes, then in the ionization region ($\rho_0 < \rho < \rho_1$), electron density is described as

$$\frac{\partial^2 n_r}{\partial \rho^2} + \frac{1}{\rho}\frac{\partial n_r}{\partial \rho} + \frac{\nu_i/p}{Dp} n_r = 0. \tag{22}$$

The general solution is

$$n_{r1}(\rho) = a_1 J_0(\gamma_1 \rho) + a_2 Y_0(\gamma_1 \rho) \tag{23}$$

where

$$\gamma_1 = \sqrt{\frac{\nu_i/p}{Dp}}. \tag{24}$$

In the attachment region ($\rho > \rho_1$), the expression for electron density is

$$\frac{\partial^2 n_r}{\partial \rho^2} + \frac{1}{\rho}\frac{\partial n_r}{\partial \rho} - \frac{\nu_a/p}{Dp} n_r = 0 \tag{25}$$

and the general solution is

$$n_{r2}(\rho) = a_3 K_0(\gamma_2 \rho) + a_4 I_0(\gamma_2 \rho) \tag{26}$$

where

$$\gamma_2 = \sqrt{\frac{\nu_a/p}{Dp}}. \tag{27}$$

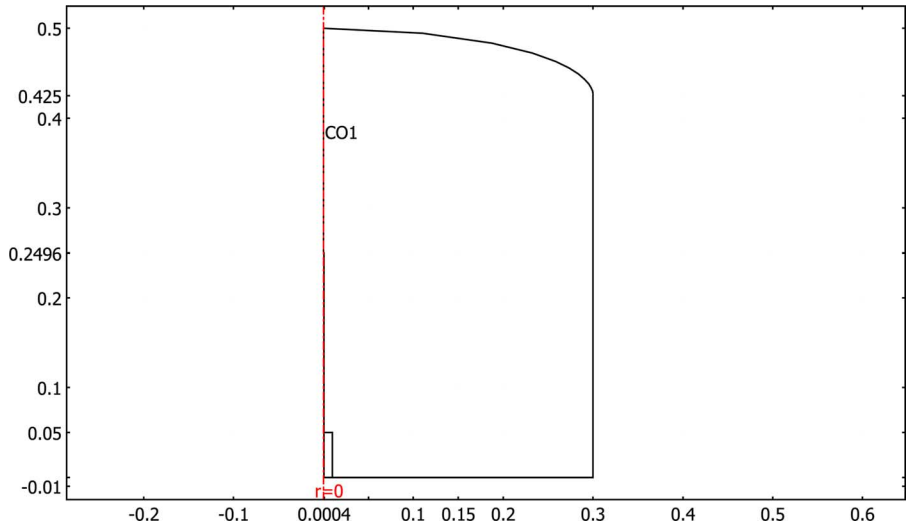

Fig. 1. Vacuum chamber geometry for the finite-element analysis.

The applicable boundary conditions are as follows:

$$\begin{aligned} n_{r1}(\rho_0) &= 0 \\ n_{r2}(\rho_2) &= 0, \qquad \text{as } \rho_2 \to \infty \\ n_{r1}(\rho_1) &= n_{r2}(\rho_1) \\ n'_{r1}(\rho_1) &= n'_{r2}(\rho_1). \end{aligned} \tag{28}$$

Solutions exist for values of γ_1 and γ_2 for which

$$\begin{vmatrix} J_0(\gamma_1\rho_0) & Y_0(\gamma_1\rho_0) & 0 & 0 \\ 0 & 0 & K_0(\gamma_2\rho_2) & I_0(\gamma_2\rho_2) \\ J_0(\gamma_1\rho_1) & Y_0(\gamma_1\rho_1) & -K_0(\gamma_2\rho_1) & -I_0(\gamma_2\rho_1) \\ J'_0(\gamma_1\rho_1) & Y'_0(\gamma_1\rho_1) & -K'_0(\gamma_2\rho_1) & -I'_0(\gamma_2\rho_1) \end{vmatrix} = 0. \tag{29}$$

From (29), it is possible to calculate the electric field strength corresponding to corona onset for a particular pressure and monopole radius.

III. Experimental Work

A. Measurement of Corona Onset at 60 Hz

Corona onset voltages were measured for a hemispherically capped monopole in a vacuum chamber as a function of pressure and temperature.

The monopole was 25 cm long with a radius of 3.8×10^{-2} cm. It was made of stainless steel with a hemispherical cap. The monopole was mounted on a ground plane 15 cm in radius. Insulating material was installed on the lower 3 cm of the monopole to prevent breakdown between the monopole and the ground plane.

The vacuum chamber was a steel bell mounted on an aluminum plate. The bell was 80 cm high at the center of the dome and 30 cm in radius. The monopole was mounted in the center of the bell's interior. The ground plane, bell, and plate were conductively bonded and referenced to the ground lead of the voltage source.

The monopole was excited with a 60-Hz source. Near the top of the monopole was an ionizing source (americium-241) that provided initial ionization for corona formation.

Before a series of measurements, the chamber, ground plane, and monopole were carefully cleaned. The monopole was repeatedly cleaned between corona events. In the preparation for a measurement, the chamber was sealed and pumped down to about 1 torr, then backfilled with air dried through a desiccant. The dry air was then pumped down to the target pressure and the chamber stabilized. Thus, the air was entirely changed between successive measurements of corona onset. Both temperature and pressure in the chamber were recorded.

The exciting voltage was stepped in increments of about 1% until corona was noted. The voltage was held at each step for 5 s or more to allow time for corona onset. With the aid of the ionizing source, corona was established in much less than a second upon reaching the corona onset voltage.

Corona onset was detected using the unaided human eye per the American National Standards Institute (ANSI) Standard C29.1 [38]. The area near the chamber's view port was thoroughly darkened and the observer's eyes were allowed to adjust to the darkness. Corona inception was consistently observed on the surface of the cylindrical section of the monopole. The radius of the corona varied inversely with pressure but did not extend to the walls or floor of the vacuum chamber.

Measurements were made at 22 pressures between 1 and 150 torr.

1) Finite-Element Analysis of Surface Electric Field: A finite-element analysis of the monopole, ground plane, and vacuum chamber was performed to correlate the excitation voltage with the electric field intensity on the surface of the monopole. Fig. 1 shows the geometry used in the analysis. The analysis was performed using COMSOL Multiphysics software [39] in an axisymmetric mode. The ratio of electric field intensity at the surface of the monopole to potential at the drive point was calculated to be 15.4 V/cm per volt.

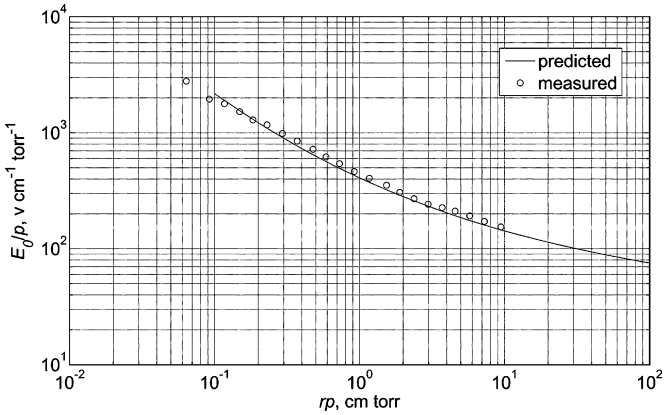

Fig. 2. Predicted and measured corona onset at 60 Hz compared.

2) Results: Fig. 2 compares the predictions of corona onset with the measurements at 60 Hz. The data are presented in proper variables, i.e., E/p in volts per centimeter torr as a function of rp in centimeter torr. The small divergence between measurement and prediction below $rp = 0.1$ cm·torr is due to granularity in the measurement of pressure.

Pressure was corrected for temperature using the formula

$$p = p_{\text{observed}} \left(\frac{288.15}{273 + T} \right) \tag{30}$$

where T is the temperature in degrees centigrade.

The results confirm that a value of the Townsend integral, $K = 3500$, is a good predictor of corona onset at 60 Hz for cylindrical geometries over the range $0.1 < rp < 10$ cm·torr.

The 60-Hz corona onset criterion predicted by (17) can be fitted to a second-order polynomial curve valid over the range $0.1 < rp < 100$ cm·torr with a correlation coefficient $R^2 = 0.999$

$$\begin{aligned} y &= 0.049x^2 - 0.587x + 6.03 \\ x &= \ln(r_0 p)\ \text{cm} \cdot \text{torr} \\ y &= \ln(E_0/p)\ \text{V/cm} \cdot \text{torr}. \end{aligned} \tag{31}$$

B. Measurement of Corona Onset at 300 MHz

Corona onset voltages were measured for the hemispherically capped monopole in a vacuum chamber as a function of pressure and temperature. The frequency 300 MHz was chosen because a monopole resonant at that frequency fit the available vacuum apparatus.

The monopole was the same as used in the measurement of corona onset at 60 Hz. The monopole was mounted on a ground plane a 70-cm square that served as the floor of the vacuum chamber. Paraffin was molded on the lower 5 cm of the monopole to prevent breakdown between the monopole and the ground plane.

The vacuum chamber was completed with a glass bell. The bell was 78 cm high at the center of the dome and 23 cm in radius. The monopole was mounted in the center of the bell's interior on the vacuum plate. The protocols for cleaning the apparatus and exchanging air were the same as used in the 60-Hz measurements.

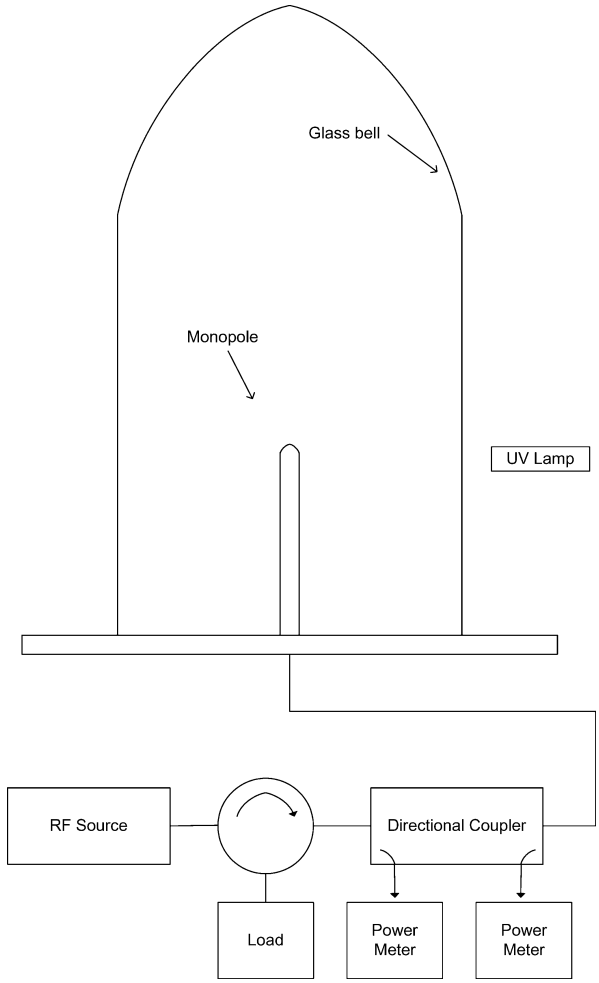

Fig. 3. Experimental apparatus.

The monopole was excited with a signal source and RF amplifier at 300 MHz (see Fig. 3). Ultraviolet illumination from a mercury vapor arc promoted electron production at the surface of the antenna. The RF excitation was increased slowly until corona was noted. With the aid of the ultraviolet source, corona was established in much less than a second upon reaching the corona onset voltage.

Corona onset was detected using the unaided human eye per ANSI Standard C29.1 [38]. The chamber was located in a darkened, shielded room and the observer's eyes were allowed to adjust to the darkness before attempting measurements. Corona inception was consistently observed along the upper 2 cm of the cylindrical portion of the monopole. The corona was quite intense but was confined within a centimeter of the monopole.

Measurements were made at 14 pressures between 5 and 100 torr.

1) Numerical Analysis of Surface Electric Field: An analysis of the monopole and ground plane was performed using the numerical electromagnetic code (NEC) [40] to correlate the antenna current distribution with the electric field intensity at the surface of the monopole. The electric field at the surface of

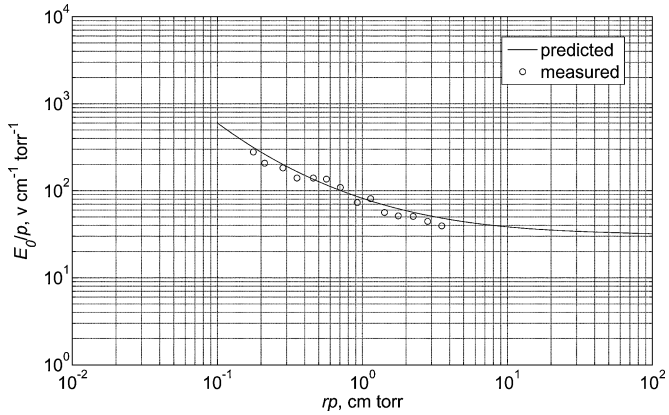

Fig. 4. Predicted and measured corona onset at 300 MHz compared.

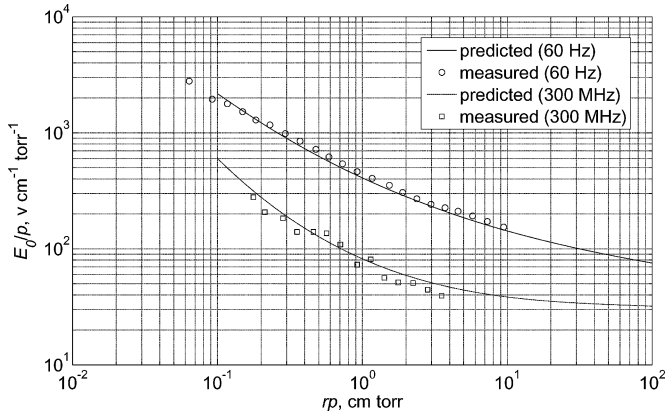

Fig. 5. Predicted and measured corona onset at 60 Hz and 300 MHz.

the monopole is dominated by the quasi-static component [35] and is calculated either from an estimate of the antenna's charge distribution or by extrapolating the calculated near electric field to the surface assuming $1/r$ dependence [22]. The ratio of the electric field intensity at the top of the monopole to the drive point current was calculated to be 2180 V/cm per ampere at 300 MHz. The drive point current was calculated from a measurement of input power and antenna impedance.

2) Results: Fig. 4 compares the predictions of corona onset with the measurements at 300 MHz. Pressure was corrected for temperature. The results confirm that at 300 MHz, the electron continuity equation with only the diffusion loss term is a good predictor of corona onset for isolated, cylindrical geometries over the range $0.1 < rp < 10$ cm·torr.

The RF corona onset criterion predicted by (29) can be fitted to a third-order polynomial curve valid over the range $0.1 < rp < 100$ cm·torr with a correlation coefficient $R^2 = 0.999$

$$\begin{aligned} y &= -0.009x^3 + 0.116x^2 - 0.549x + 4.41 \\ x &= \ln(r_0 p)\ \text{cm} \cdot \text{torr} \\ y &= \ln(E_0/p)\ \text{V/cm} \cdot \text{torr}. \end{aligned} \tag{32}$$

Predicted and measured corona onset for both 60 Hz and 300 MHz are compared in Fig. 5. As rp increases, the two criteria asymptotically approach $E/p \approx 32$ V/cm·torr.

IV. Transition Frequency

As early as 1915, Ryan and Marx [41] noted that the corona onset voltage for nonuniform fields was significantly lower at 100 kHz than at 60 Hz though they did not explain the difference. Brown and MacDonald [17] described limits to the diffusion theory of microwave breakdown, one of which may explain a transition from drift-controlled corona onset to diffusion-controlled corona onset as frequency is increased from 60 Hz. They described an *oscillation amplitude limit* that applies when an electron drifts from its point of origin to the walls of the cavity or vacuum chamber in a half-cycle. Since the electric field is both time-varying and nonuniform, the calculation of this limit for a particular application is not simple. A first-order estimate is obtained for the steel bell used in the 60-Hz measurements by noting that electron drift is on the order of 10^7 cm/s [42] and that the radius of the chamber is 30 cm, yielding a nominal transit time of 3×10^{-6} s. Thus, at frequencies less than about 170 kHz, electron loss by drift to the walls might be expected.

If, however, the monopole is truly isolated, drift might affect corona onset. To the degree that electrons are transported past the ionization boundary during a portion of the excitation cycle, they cease momentarily to contribute to ionization. A calculation of electron motion using the electron drift velocity data of Ryzko [42] shows electrons in our experiment drifted outside the region of ionization for values of $rp > 3$ cm·torr although no marked change in corona onset was observed.

If, however, electrons that drift across the ionization boundary were never to return, the effect on corona onset could be similar to that ascribed to the oscillation amplitude limit. In the air outside the ionization boundary, the only potential electron loss mechanisms are recombination or attachment. Since few positive ions exist before corona onset, attachment would seem to be the sole candidate of electron loss.

Chanin *et al.* [43] explain that at electron energies greater than about 1 eV ($E/p > 4$ V/cm·torr), two-body attachment processes dominate in air, both radiative and dissociative

$$\begin{aligned} &e + \mathrm{O_2} \rightarrow \mathrm{O_2^-} + h\nu \text{ or} \\ &e + \mathrm{O_2} \rightarrow (\mathrm{O_2^-})_{\mathrm{unstable}} \rightarrow \mathrm{O} + \mathrm{O^-} + \text{kinetic energy}. \end{aligned} \tag{33}$$

But at electron energies less than 1 eV, three-body attachment processes dominate in air, e.g.,

$$e + \mathrm{O_2} + \mathrm{O_2} \rightarrow \mathrm{O_2^-} + \mathrm{O_2^*}. \tag{34}$$

Furthermore, they state that while the attachment coefficient η/p is not a function of pressure for average electron energies above 1 eV, it is a function of molecular oxygen density squared below 1 eV. Truby [44] has measured the three-body electron attachment coefficient k for $\mathrm{O_2}$ and shown that it is insensitive to electron energy but is a function of gas temperature, as shown in Table I.

The time dependence of electron density due to attachment is [44]

$$\frac{\partial n}{\partial t} = -k\,[\mathrm{O}]^2\, n \tag{35}$$

TABLE I
THREE-BODY ELECTRON ATTACHMENT COEFFICIENT FOR OXYGEN

Temperature, °K	k, $\mathrm{cm}^6\ \mathrm{s}^{-1}$
113	7.2×10^{-31}
200	1.5×10^{-30}
300	2.1×10^{-30}

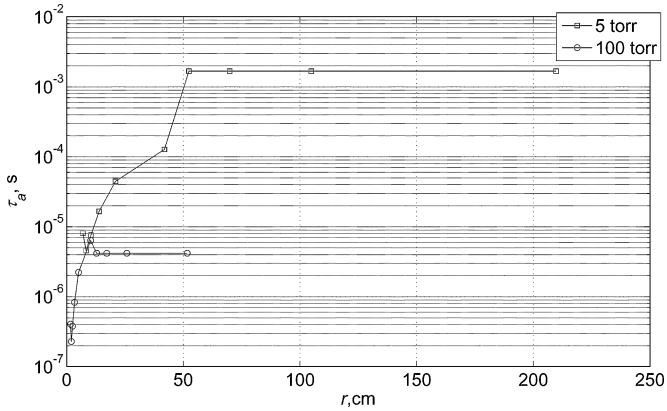

Fig. 6. Characteristic time of attachment for the experiment.

where $[\mathrm{O}]^2$ is the number density of molecular oxygen and n is the electron number density. In a source-free region, electron density will behave as

$$n = n_0\, e^{-k[\mathrm{O}]^2 t} = n_0\, e^{-t/\tau_a} \tag{36}$$

where n_0 is an initial electron density and τ_a is the characteristic time of attachment.

Using the electron attachment data of Chatterton and Craggs [45], the electron drift measurements of Ryzko [42], and the three-body electron attachment coefficients of Truby [44], we calculated the characteristic times of attachment as a function of distance from the monopole (see Fig. 6) for the two extreme pressures of the 300-MHz measurement. It is seen to vary from about 10^{-7} to 10^{-3} s. But, because the drift velocity is more nearer the monopole owing to the higher electric field, electrons will pass the ionization boundary and the region of the two-body attachment in about 10^{-7} s or less and slow as they enter the region of the three-body attachment. Attachment outside the ionization boundary is dominated by three-body processes.

If one assumes that near-total loss of electrons by attachment will have an effect indistinguishable from loss of electrons by drift to the walls of the vacuum chamber or cavity, then that frequency f_c for which a half-cycle corresponds to $3\tau_a$ (a 95% loss) may be a good indicator of transition between drift-controlled corona onset and diffusion-controlled corona onset. Table II shows the calculated estimates of transition frequency for the two extreme pressures in the 300-MHz experiment as well as for conditions in flight [46].

TABLE II
ESTIMATED TRANSITION FREQUENCY

	p, torr	$[\mathrm{O}_2]$, cm^{-3}	τ_a, s	f_c, Hz
Experiment	4.6	3.28×10^{16}	4.65×10^{-4}	360
Experiment	92.5	6.55×10^{17}	1.17×10^{-6}	143 000
40 000 ft.	187	1.33×10^{18}	3.78×10^{-7}	440 000

V. CONCLUSION

Measurements of corona onset for an isolated cylindrical monopole at both power frequency and RF are in good agreement with predictions developed from the electron continuity equation over a large range of air density and cylinder radius.

The frequency at which drift-controlled corona onset changes to diffusion-controlled corona onset may be a function of electron attachment outside the ionization boundary. If so, estimates of a transition frequency are made for our isolated monopole. The transition has not been observed experimentally and remains an object of future research.

Since most instances of corona on aircraft involve nonuniform fields, the criteria reported here have been very useful in creating corona-free designs for antennas and transmission lines in high-power RF systems. The criteria have also proved useful in scaling pressure and electric field intensity for the purposes of test.

APPENDIX

The electron continuity equation (4) can be solved, in principle, by separation of variables. Let

$$n(r,t) = n_r(r) n_t(t). \tag{37}$$

The electron continuity equation then becomes

$$n_r \frac{\partial n_t}{\partial t} = n_t g(n_r, r) + \nu n_r n_t \tag{38}$$

where g is a differential function in r. Separating spatial and temporal variables, the electron continuity equation is

$$\frac{n_t'}{n_t} = \frac{g(n_r, r)}{n_r} + \nu = \lambda. \tag{39}$$

The time-dependent function is

$$n_t = e^{\lambda t}. \tag{40}$$

Herlin and Brown [14] demonstrated that before an electric field is applied, λ assumes characteristic values that are all negative and the electron density tends to zero. As the electric field is increased, the characteristic values become less negative until one equals zero. At that point, electron production by ionization equals electron loss through drift, diffusion, and convection. As the field is increased slightly more, one characteristic value becomes positive and electron density increases exponentially. Thus, corona onset corresponds to $\lambda = 0$ and is described by the solution to the homogeneous differential equation

$$g(n_r, r) + \nu n_r = 0. \tag{41}$$

ACKNOWLEDGMENT

The authors are grateful for the kind assistance of Dr. R. Fante.

REFERENCES

[1] R. H. Marriot, "Radio range variation," in *Proc. IRE*, Mar. 1914, vol. 2, no. 3, pp. 37–53.
[2] W. Price, D. Thiel, J. Drapala, and R. Olsen, "Corona onset voltage at 60 hertz for an isolated, cylindrical electrode," in *Proc. 2006 IEEE Int. Symp. Electromagn. Compat.*, vol. 2, pp. 333–336.
[3] W. Price, D. Thiel, J. Drapala, and R. Olsen, "Corona onset voltage at high frequency for an isolated, cylindrical electrode," in *Proc. 2007 IEEE Int. Symp. Electromagn. Compat.*, pp. 1–4.
[4] J. S. Townsend, *Electricity in Gases*, 1st ed. London: Oxford Univ. Press, 1915.
[5] L. B. Loeb, "The threshold for the positive pre-onset burst pulse corona and the production of ionizing photons in air at atmospheric pressure," *Phys. Rev.*, vol. 73, no. 7, pp. 798–800, 1948.
[6] J. S. Townsend, *Electrons in Gases*. London, U.K.: Hutchinson, 1947.
[7] D. B. Phillips, R. G. Olsen, and P. D. Pedrow, "Corona onset as a design optimization criterion for high voltage hardware," *IEEE Trans. Dielectr. Electr. Insul.*, vol. 7, no. 6, pp. 744–751, Dec. 2000.
[8] I. McAllister and A. Pedersen, "Corona-onset field-strength calculations and the equivalent radius concept," *Arch. Elektrotechnik*, vol. 64, pp. 43–48, 1981.
[9] M. P. Sarma and W. Janischewskyj, "D.C. corona on smooth conductors in air," *Proc. Inst. Electr. Eng.*, vol. 116, no. 1, pp. 161–166, 1969.
[10] P. D. Pedrow and R. G. Olsen, "Corona streamer onset as an optimization criterion for design of high voltage hardware on transmission lines," in *Proc. 1996 IEEE Int. Symp. Electr. Insul.*, Montreal, CA, 1996, pp. 312–315.
[11] R. Buderi, *The Invention that Changed the World*. New York: Simon & Schuster, 1996.
[12] H. Mehlhardt, "The electric strength of antenna installations in airplanes operating at high altitudes," Air Materiel Command, Wright-Patterson Air Force Base, OH, Tech. Rep. F-TS-1106-RE, 1937.
[13] D. Q. Posin, "The microwave spark," *Phys. Rev.*, vol. 73, no. 5, pp. 496–509, 1948.
[14] M. A. Herlin and S. C. Brown, "Breakdown of a gas at microwave frequencies," *Phys. Rev.*, vol. 74, no. 3, pp. 291–296, 1948.
[15] M. A. Herlin and S. C. Brown, "Electrical breakdown of a gas between coaxial cylinders at microwave frequencies," *Phys. Rev.*, vol. 74, no. 8, pp. 910–913, 1948.
[16] M. A. Herlin and S. C. Brown, "Microwave breakdown of a gas in a cylindrical cavity of arbitrary length," *Phys. Rev.*, vol. 74, no. 11, pp. 1650–1656, 1948.
[17] S. C. Brown and A. D. MacDonald, "Limits for the diffusion theory of high frequency gas discharge breakdown," *Phys. Rev.*, vol. 76, no. 11, pp. 1629–1634, 1949.
[18] W. P. Allis and S. C. Brown, "High frequency electrical breakdown of gases," *Phys. Rev.*, vol. 87, no. 3, pp. 419–424, 1952.
[19] J. Chown, T. Morita, and W. Scharfman, "Voltage breakdown characteristics of microwave antennas," in *Proc. IRE Int. Conv. Rec.*, 1958, vol. 6, p. 199.
[20] J. Chown, T. Morita, and W. Scharfman, "Voltage breakdown characteristics of microwave antennas," in *Proc. IRE*, 1959, pp. 1331–1337.
[21] W. Scharfman and T. Morita, "Power-handling capability of antennas at high altitude," in *Proc. IRE Int. Conv. Record*, 1960, vol. 8, pp. 103–114.
[22] W. Scharfman and T. Morita, "Voltage breakdown of antennas at high altitudes," Stanford Res. Inst., Stanford, CA, Tech. Rep. 69, Apr. 1960.
[23] W. Scharfman, W. C. Taylor, and T. Morita, "Research study of microwave breakdown of air at high altitudes," Air Force Cambridge Res. Lab., Cambridge, MA, Tech. Rep. AFCRL-62-732, Aug. 1962.
[24] W. C. Taylor, W. Scharfman, and T. Morita, "Voltage breakdown of microwave antennas," in *Advances in Microwaves*, vol. 7, L. Young, Ed. New York: Academic, 1971, pp. 59–130.
[25] G. August, J. B. Chown, and W. C. Taylor, "Power-handling capability of ECM antennas," Air Force Systems Command, MD, Tech. Rep. AD-751 309, Sep. 1972.
[26] R. Fante, "Mathematical analysis of microwave breakdown in flowing gases," *IEEE Trans. Antennas Propag.*, vol. AP-13, no. 5, pp. 781–788, Sep. 1965.
[27] R. Fante and J. Mayhan, "Bounds on the electric field outside a radiating system," *IEEE Trans. Antennas Propag.*, vol. AP-16, no. 6, pp. 712–717, Nov. 1968.
[28] R. Fante and J. T. Mayhan, "Microwave breakdown predictions for a rectangular aperture antenna," *J. Appl. Phys.*, vol. 40, no. 12, pp. 4750–4752, 1969.
[29] J. T. Mayhan and R. Fante, "Microwave breakdown over a semi-infinite interval," *J. Appl. Phys.*, vol. 40, no. 13, pp. 5207–5211, 1969.
[30] R. Fante and J. Mayhan, "Bounds on the electric field outside a radiating system—II," *IEEE Trans. Antennas Propag.*, vol. AP-18, no. 1, pp. 64–68, Jan. 1970.
[31] R. Fante and J. M. Yos, "Breakdown in the near field of re-entry vehicle antennas," Air Force Cambridge Res. Lab., Cambridge, MA, Tech. Rep. AFCRL-71-0228, Apr. 1971.
[32] R. L. Fante, J. M. Yos, and J. J. Otazo, "Simple analytical models for calculating breakdown in air-filled transmission systems," Air Force Cambridge Res. Lab., Cambridge, MA, Tech. Rep. AFCRL-71-0206, Apr. 1971.
[33] J. T. Mayhan, R. L. Fante, R. O'Keefe, R. Elkin, J. Klugerman, and J. M. Yos, "Comparison of various microwave breakdown prediction models," *J. Appl. Phys.*, vol. 42, no. 13, pp. 5362–5369, 1971.
[34] J. M. Yos, "Microwave breakdown predictions for a rectangular aperture antenna including lateral diffusion," Air Force Cambridge Res. Lab., Cambridge, MA, Tech. Rep. AFCRL-71-0120, Feb. 18 1971.
[35] S. A. Schelkunoff and H. T. Friis, *Antennas, Theory and Practice.* Applied Mathematics Series. New York: Wiley, 1966.
[36] G. Francis, *Ionization Phenomena in Gases*. London: Butterworths Scientific Publications, 1960.
[37] S. C. Brown, *Introduction to Electrical Discharges in Gases.* Wiley Series in Plasma Physics. New York: Wiley, 1966.
[38] American National Standards Institute, "ANSI standard for electrical power insulators-test methods," Amer. Nat. Standards Inst., Washington, DC, Tech. Rep. C29.1–1988, Aug. 23, 1988.
[39] COMSOL "COMSOL multiphysics," presented at the COMSOL Proc., Cambridge, MA, 2005.
[40] G. A. Burke and A. J. Poggio, "Numerical electromagnetics code (NEC)—Method of Moments, Parts I, II, III," Lawrence Livermore Nat. Lab., Livermore, CA, Tech. Doc. 116, 1981.
[41] H. J. Ryan and R. G. Marx, "Sustained radio frequency high voltage discharges," in *Proc. IRE*, 1915, vol. 3, no. 4, pp. 349–365.
[42] H. Ryzko, "Drift velocity of electrons and ions in dry and humid air and in water vapour," in *Proc. Phys. Soc.*, 1965, vol. 85, pp. 1283–1295.
[43] L. M. Chanin, A. V. Phelps, and M. A. Biondi, "Measurements of the attachment of low-energy electrons to oxygen molecules," *Phys. Rev.*, vol. 128, no. 1, pp. 219–230, 1962.
[44] F. K. Truby, "Low-temperature measurements of the three-body electron-attachment coefficient in O2," *Phys. Rev. A*, vol. 6, no. 2, pp. 671–676, 1972.
[45] P. A. Chatterton and J. D. Craggs, "Attachment coefficient measurements in carbon dioxide, carbon monoxide, air and helium-oxygen mixtures," *Proc. Phys. Soc.*, vol. 85, no. 2, pp. 355–362, 1965.
[46] "U.S. Standard Atmosphere, 1976," Nat. Oceanic and Atmos. Admin., Nat. Aeronaut. Space Admin., U.S. Air Force, Tech. Rep. NOAA-S/T 76-1562, Oct. 1976.

William O. Price (M'75) received the B.S. degree in electrical and computer engineering from Oregon State University, Corvallis, in 1975, and the M.S. degree in electrical engineering from California State University, Northridge, in 1976. He is currently working toward the Ph.D. degree at Griffith University, Brisbane, Qld., Australia.

From 1975 to 1987, he was with the Naval Air Systems Command, Pacific Missile Test Center, Pt. Mugu, CA. Since 1987, he has been with Boeing Company, Seattle, WA, where he is currently a Technical Fellow in the Airborne Warning Systems Division.

John Drapala (M'01) received the B.S. degree in electrical engineering from Seattle Pacific University, Seattle, WA, in 1998.

From 1978 to 1986, he was with the U.S. Air Force. Since 1986, he has been with the Airborne Warning Systems Division, Boeing Company, Seattle.

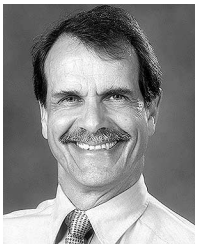

David V. Thiel (M'81–SM'88) received the B.Sc. degree from the University of Adelaide, Adelaide, Australia, in 1970, and the M.Sc. and Ph.D. degrees from James Cook University, Townsville, Australia, in 1974 and 1980, respectively, all in electrical engineering.

He is currently a Professor in the Griffith School of Engineering, Griffith University, Brisbane, Qld., Australia, where he is also the Director of the Centre for Wireless Monitoring and Applications. He worked with the team that developed the world's first odor-sensing robot. He lead the development of the Thiel surface impedance method, a surface impedance meter used in Central Queensland coalfields for premining coal seam assessment. His current research interests include smart antennas, numerical modeling in electromagnetics, electromagnetic geophysics, and integrated sensor and packaging technologies.

Prof. Thiel is a Fellow of the Engineers Australia. He was the Chair of the Wave Propagation Standards Committee of the IEEE Antennas and Propagation Society and currently a member of the Antennas Standards Committee.

Robert G. Olsen (S'66–F'92) received the B.S. degree in electrical engineering from Rutgers University, New Brunswick, NJ, in 1968, and the M.S. and Ph.D. degrees in electrical engineering from the University of Colorado, Boulder, in 1970 and 1974, respectively.

He is currently an Associate Dean of the College of Engineering and Architecture and the Boeing Distinguished Professor of Electrical Engineering, Washington State University (WSU), Pullman. Since 1973, he has been a member of the electrical engineering faculty at WSU. During that time, he has been a Visiting Scientist at general telephone and electronics (GTE) Laboratories, Waltham, MA; at ABB Corporate Research, Västeras, Sweden; and at the Electric Power Research Institute, Palo Alto, CA, and a Visiting Professor at the Technical University, Denmark. His current research interests include electromagnetic interference from power lines, the electromagnetic environment of power lines, electromagnetic wave propagation, electromagnetic compatibility, and electromagnetic scattering. His work in these areas has resulted in many publications in refereed journals.

Dr. Olsen is an Honorary Life Member of the IEEE Electromagnetics Compatibility Society. He is the past Technical Editor of the IEEE Electromagnetic Compatibility Society Newsletter, the past U.S. National Committee Representative to the international council on large electric systems (CIGRE) Study Committee 36 (electromagnetic compatibility), and past Chair of the IEEE Power Engineering Society AC Fields and Corona Effects Working Groups. He is also a past Associate Editor of the IEEE TRANSACTIONS ON ELECTROMAGNETIC COMPATIBILITY and *Radio Science*. His most recent work has been supported by the Bonneville Power Administration, Boeing Integrated Defense Systems, the Electric Power Research Institute, the National Science Foundation, and the U.S. Navy.